HHS Public Access

Author manuscript

Cell Rep. Author manuscript; available in PMC 2022 September 14.

Published in final edited form as:

Cell Rep. 2022 August 23; 40(8): 111239. doi:10.1016/j.celrep.2022.111239.

Central FGF21 production regulates memory but not peripheral metabolism

Bolu Zhou[1,2,3], **Kristin E. Claflin**[1,2,3], **Kyle H. Flippo**[1,2,3], **Andrew I. Sullivan**[1,2,3], **Arvand Asghari**[1,2,3], **Satya M. Tadinada**[1,3], **Sharon O. Jensen-Cody**[1,2,3], **Ted Abel**[1,3], **Matthew J. Potthoff**[1,2,3,4,5,*]

[1]Department of Neuroscience and Pharmacology, University of Iowa Carver College of Medicine, 169 Newton Road, 3322 PBDB, Iowa City, IA 52242, USA

[2]Fraternal Order of Eagles Diabetes Research Center, University of Iowa Carver College of Medicine, 169 Newton Road, 3322 PBDB, Iowa City, IA 52242, USA

[3]Iowa Neurosciences Institute, University of Iowa Carver College of Medicine, 169 Newton Road, 3322 PBDB, Iowa City, IA 52242, USA

[4]Department of Veterans Affairs Medical Center, Iowa City, IA 52242, USA

[5]Lead contact

SUMMARY

Fibroblast growth factor 21 (FGF21) is a liver-derived endocrine hormone that functions to regulate energy homeostasis and macronutrient intake. Recently, FGF21 was reported to be produced and secreted from hypothalamic tanycytes, to regulate peripheral lipid metabolism; however, rigorous investigation of FGF21 expression in the brain has yet to be accomplished. Using a mouse model that drives CRE recombinase in FGF21-expressing cells, we demonstrate that FGF21 is not expressed in the hypothalamus, but instead is produced from the retrosplenial cortex (RSC), an essential brain region for spatial learning and memory. Furthermore, we find that central FGF21 produced in the RSC enhances spatial memory but does not regulate energy homeostasis or sugar intake. Finally, our data demonstrate that administration of FGF21 prolongs the duration of long-term potentiation in the hippocampus and enhances activation of hippocampal neurons. Thus, endogenous and pharmacological FGF21 appear to function in the hippocampus to enhance spatial memory.

Graphical Abstract

*Correspondence: matthew-potthoff@uiowa.edu.

AUTHOR CONTRIBUTIONS

B.Z., K.E.C., K.H.F., A.I.S., S.O.J., and A.A. designed and performed experiments and interpreted the data. S.M.T. performed hippocampal LTP recordings. B.Z. and K.E.C. wrote the manuscript. S.M.T. and T.A. interpreted the electrophysiology data and contributed to the written manuscript. M.J.P. conceived the project, designed experiments, interpreted data, and wrote the manuscript and is responsible for the integrity of its content.

SUPPLEMENTAL INFORMATION

Supplemental information can be found online at https://doi.org/10.1016/j.celrep.2022.111239.

DECLARATION OF INTERESTS

The authors declare no competing interests.

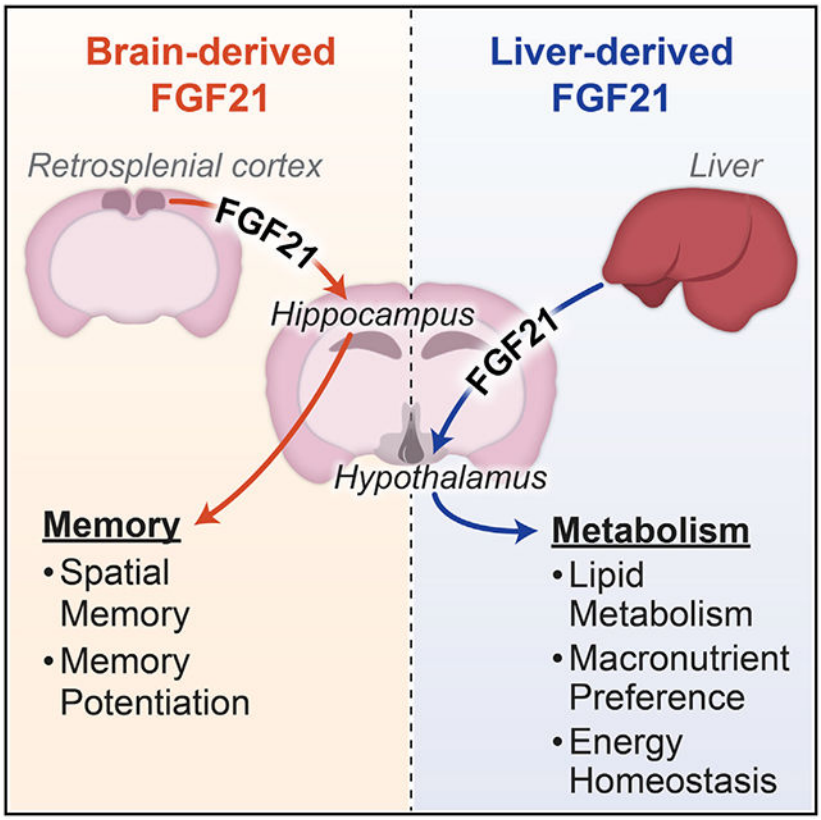

In brief

Zhou et al. reveal that the endocrine hormone FGF21 is expressed in the brain. Central FGF21 expression occurs in distinct areas, including the retrosplenial cortex, but not the hypothalamus. Interestingly, brain-derived FGF21 regulates spatial memory formation, but not metabolism, and the converse is true for liver-derived FGF21.

INTRODUCTION

Fibroblast growth factor 21 (FGF21) is a member of the FGF family that exhibits numerous metabolic functions to maintain energy homeostasis and regulate macronutrient intake (BonDurant and Potthoff, 2018; Fisher and Maratos-Flier, 2016). FGF21 signals through a cell surface receptor complex composed of a classic FGF receptor, FGFR1c, and the obligate FGF co-receptor, β-klotho (KLB) (Adams et al., 2012; Ding et al., 2012; Kurosu et al., 2007; Wu et al., 2007). While circulating FGF21 is derived primarily from the liver, *Fgf21* mRNA expression is detected in multiple tissues, including the pancreas, adipose tissues, thymus, gastrointestinal tract, and brain (Fon Tacer et al., 2010; Markan et al., 2014; Owen et al., 2015). The level of FGF21 expression within any particular tissue can change markedly in response to energy status (i.e., high carbohydrate or low protein) or metabolic challenges (e.g., nutrient deprivation or overfeeding) (Flippo and Potthoff, 2021). Circulating FGF21 crosses the blood-brain barrier and signals through its receptor complex expressed in different regions of the central nervous system (CNS) to regulate energy

homeostasis (i.e., promote weight loss or influence macronutrient preference) (Ameka et al., 2019; Flippo et al., 2020, 2022; Jensen-Cody et al., 2020; Owen et al., 2014).

A recent study suggests that FGF21 can be produced and secreted from hypothalamic tanycytes, a specialized population of ependymogial cells that line the third ventricle (Geller et al., 2019). The same study reported that knockdown of FGF21 from the hypothalamus promoted lipolysis and energy expenditure through paracrine actions of FGF21 on other hypothalamic regions (Geller et al., 2019). Using knockin reporter mice that express CRE recombinase under the control of the endogenous FGF21 promoter, we demonstrate here that in fact FGF21 is not expressed in tanycytes or the hypothalamus but is instead expressed in a few brain regions including the retrosplenial cortex (RSC) and thalamus. In addition, acute deletion of FGF21 in neurons does not influence energy homeostasis or sweet taste preference, but instead affects spatial memory. Importantly, we found that pharmacological administration of FGF21 had both short- and long-term effects on spatial memory formation, consolidation, and recall. These effects of FGF21 are supported by enhanced long-term potentiation (LTP) following acute treatment of hippocampal slices with FGF21. Taken together, we reveal that FGF21 increases the consolidation of spatial memory formation and that RSC-derived FGF21 is important for spatial memory formation.

RESULTS

FGF21 is expressed in the RSC and thalamus

To comprehensively assess the tissue and cellular distribution of FGF21, we used CRISPR to generate *Fgf21*-P2A-CRE mice, which have a viral 2A oligopeptide that mediates ribosomal skipping and a CRE recombinase gene inserted immediately downstream of the FGF21 stop codon (Figure 1A). As expected, CRE expression in *Fgf21*-P2A-CRE mice recapitulates the known expression and induction of *Fgf21* mRNA expression in the liver in response to fasting (Figures S1A and S1B). These mice were subsequently crossed to CRE-dependent Ai14-tdTomato reporter mice (*Fgf21*-CRE; Ai14-tdTomato) to identify cells that have ever expressed FGF21. *Fgf21*-CRE; Ai14-tdTomato mice exhibited abundant tdTomato signal in both the liver (Figure 1B) and the pancreas (Figure S1C), tissues known to exhibit high levels of FGF21 mRNA and protein (Fon Tacer et al., 2010). Importantly, and in contrast to a previous report (Geller et al., 2019), no cells in the median eminence or third ventricle in the hypothalamus were positive for tdTomato in male (Figure 1C) or female *Fgf21*-CRE; Ai14-tdTomato mice (Figure S1D). Notably and unexpectedly, we observed numerous tdTomato-positive cells in the thalamic nucleus and RSC of *Fgf21*-CRE; Ai14-tdTomato, but not CRE negative (Ai14-tdTomato only) mice (Figure 1C). RNAscope *in situ* hybridization for *Fgf21* and *tdTomato* mRNAs confirmed that tdTomato expression in *Fgf21*-CRE; Ai14-tdTomato mice is specific for cells that express *Fgf21* mRNA in the RSC (Figure S1E). Consistent with the *Fgf21*-CRE; Ai14-tdTomato reporter mice, no *Fgf21* mRNA was observed in the hypothalamus by *in situ* hybridization (Figure S1E). Finally, to comprehensively evaluate FGF21 expression in the CNS, we performed fDISCO clearing and imaging of brains from *Fgf21*-CRE; Ai14-tdTomato mice. Notably, we observed a significant number of $FGF21^{+}$ neurons in the RSC, cerebellum, and entorhinal cortex, but none in the hypothalamus (Video S1).

To determine locations of active FGF21 production, we injected *Fgf21*-P2A-CRE mice with a PHP.eB pAAV-FLEX-tdTomato virus that labels cells throughout the CNS that express CRE recombinase (Chan et al., 2017). Consistent with *Fgf21*-P2A-CRE; Ai14-tdTomato mice, *Fgf21*-P2A-CRE mice infected with PHP.eB pAAV-FLEX-tdTomato virus exhibited tdTomato expression in the thalamic nuclei and RSC but no expression was observed in the median eminence (Figure 1C). To investigate whether we could recapitulate the findings reporting FGF21 expression in tanycytes, we performed the same immunohistochemistry staining protocol reported by Geller et al. for FGF21 and the tanycyte marker, vimentin, using whole-body FGF21 knockout mice and wild-type controls fasted for 24 h (Geller et al., 2019). Similar to Geller et al., we observed immunofluorescence for FGF21 in the median eminence and arcuate nucleus that co-localized with vimentin. However, a similar signal was observed in controls which were stained only with secondary antibody (Figures 1D and S1F). Furthermore, this immunofluorescence associated with the FGF21 primary antibody was also present in sections from FGF21 knockout mice (Figure 1D). Overall, these results suggest previously reported observation of FGF21 expression in the median eminence and third ventricle was likely a consequence of non-specific antibody binding. These data are consistent with our observations from *Fgf21*-CRE; Ai14-tdTomato mice that FGF21 is not expressed in tanycytes within the hypothalamus. Taken together, these results indicate that FGF21 is expressed in select regions of the brain including the thalamic nuclei and RSC but not the hypothalamus.

To confirm and extend our results from *Fgf21*-P2A-CRE mice, we investigated expression of FGF21 within the brain from published single-cell RNA sequencing (RNA-seq) datasets (Campbell et al., 2017; Chen et al., 2017; Saunders et al., 2018) using the single-cell analysis R package Seurat (v3.1). Consistent with our data from *Fgf21*-P2A-CRE mice, *Fgf21* mRNA transcripts were detected in thalamic nuclei (Figure 1E), and these cells were identified as neurons by single-cell RNA-seq (Figures 1E and S1H). Importantly, consistent with our FGF21-tdTomato images, FGF21 expression was not detected in any cells that also expressed markers of tanycytes (Figures 1E, S1G, and S1H). Together, these data indicate that FGF21 is expressed in neurons of thalamic nuclei but not in hypothalamic tanycytes.

FGF21 produced from the liver, but not the CNS, regulates energy homeostasis and macronutrient balance

To determine the functional importance of central FGF21 in the regulation of energy and macronutrient homeostasis, we ablated FGF21 selectively from neurons within the CNS by injecting 4- to 8-week-old $FGF21^{fl/fl}$ mice with a PHP.eB virus expressing CRE recombinase under the control of a neuron-specific promoter (pENN.AAV.hSyn.HI.eGFP-CRE.WPRE.SV40). This approach allows for acute, neuron-specific deletion of FGF21, limiting concerns of developmental compensation observed in transgenic mice that drive constitutive CRE expression (Harno et al., 2013). Injection of the PHP.eB-CRE virus significantly induced CRE expression within the CNS including the hypothalamus and the RSC (Figures 2A, 2B, and S2A). Acute deletion of central FGF21 did not affect sucrose intake (Figure 2C) or fasting plasma ketone levels (Figure 2D), processes that FGF21 has previously been shown to regulate (Potthoff et al., 2009; von Holstein-Rathlou et al., 2016). In contrast, acute deletion of FGF21 from the liver, through administration of AAV viruses

expressing either CRE recombinase or a control construct under a liver-specific promoter (AAV-TBG-CRE and AAV-TBG-Con, respectively) to FGF21$^{fl/fl}$ mice (Figures 2E and 2F), significantly increased sucrose intake (Figures 2G and S2B) and decreased fasting ketone levels (Figure 2H). This is consistent with previous work describing a role for liver-derived FGF21 in regulating macronutrient preference and hepatic metabolism (BonDurant and Potthoff, 2018). However, consistent with a recent study (Sostre-Colon et al., 2022), we observed no differences in plasma glucose or non-esterified fatty acid (NEFA) levels in mice in which FGF21 was acutely deleted from the liver (Figures S2C and S2D).

In addition to no changes in macronutrient preference or ketone production in response to central FGF21 deletion, we also observed no changes in body weight (Figure 2I), food intake (Figure 2J), plasma glucose (Figure 2K), plasma triglycerides (Figure 2L), and energy expenditure (Figures 2M and 2N) following central FGF21 deletion. Generalized linear modeling to determine the influence of body mass on energy balance (Mina et al., 2018) also revealed that energy expenditure was unaltered in both the light and dark cycles in FGF21$^{fl/fl}$;PHP.eB-CRE mice compared with FGF21$^{fl/fl}$;PHP.eB-GFP control mice (Figures S2E and S2F). Together, these data reveal that in contrast to liver-derived FGF21, central FGF21 production is not necessary for the regulation of sugar intake or energy homeostasis.

FGF21 in the RSC is essential for spatial memory in mice

Multiple brain regions, including the hippocampus and the RSC, are important for various aspects of memory. The RSC is a hub interconnected with the prefrontal cortex, hippocampus, and thalamic nuclei (Czajkowski et al., 2014), and is also critical for spatial learning and memory (Todd et al., 2019). Given that FGF21 is expressed in the RSC, we next investigated whether central neuronal FGF21 is important for spatial learning and memory using the Barnes maze, a well-established model of hippocampal-dependent spatial memory (Patil et al., 2009). The Barnes maze consists of four training days to assess spatial learning followed by recall testing trials to evaluate memory. Central neuronal FGF21 ablation significantly impaired spatial learning and short-term memory, demonstrated by longer escape latency to locate the escape chamber during training phase and test trial (Figures 3A, S3A, and S3B). In contrast, acute deletion of FGF21 from the liver with the AAV-TBG-CRE had no effect on learning and memory (Figures 3B, S3C, and S3D).

We next examined whether FGF21 specifically in the RSC is necessary for maintaining spatial learning and memory. To do so, we reduced FGF21 expression in the RSC by injecting AAV-CMV-CRE or a control AAV-CMV-GFP virus into the RSC of FGF21$^{fl/fl}$ mice (Figure S3E). Four weeks after injection, FGF21$^{fl/fl}$;AAV-CMV-CRE and FGF21$^{fl/fl}$;AAV-CMV-GFP mice spatial memory and learning was evaluated using the Barnes maze. Delivery of the AAV-CMV-CRE to the RSC of FGF21$^{fl/fl}$ mice did not alter performance during the training phase of the Barnes maze (Figures S3F and S3G). However, during the memory testing phase, FGF21 deletion in the RSC impaired memory performance after 24 h, day 7, and day 14, as indicated by an increased latency to find the location of the escape hole relative to control mice (Figures 3C–3E). Importantly, wild-type mice administered the AAV-CMV-CRE virus in the RSC showed similar performance to control mice administered the AAV-CMV-GFP (Figures S3H–S3J). These data demonstrate

that FGF21 in the RSC contributes to maintaining spatial memory but does not contribute to spatial learning.

To confirm and extend these findings, we repeated the above experiment, but instead administered an AAV-hSyn-CRE-GFP or control virus to the RSC of $FGF21^{fl/fl}$ mice to examine the role of FGF21 in neurons in the RSC (Figure S3K). Consistent with the AAV-CMV-CRE results, administration of the AAV-hSyn-CRE virus to the RSC of $FGF21^{fl/fl}$ mice did not alter performance during the training phase of the Barnes maze (Figures S3L and S3M), but instead impaired memory performance after 24 h, day 7, and day 14 (Figures 3F–3H).

We next examined whether pharmacological FGF21 treatment affects spatial learning and memory. Memory was assessed using the Barnes maze with wild-type male mice receiving intraperito-neal (IP) injection of FGF21 1 h before the training trial each day only during the training period. We observed no difference between FGF21-treated and saline-treated control mice when assessing performance during the training period (Figures S3N and S3O); however, mice treated with FGF21 showed a significantly shorter escape latency on day 7 of the memory recall phase compared with saline-treated mice (Figure 3I). Notably, FGF21-treated mice continued to exhibit improved performance for 21 days following the last administration of FGF21 during the training period (Figure 3J), an effect that was no longer significant 28 days following the last administration (Figures 3K and 3L). However, the effect of pharmacological FGF21 in spatial memory formation was not observed in female wild-type mice, suggesting the role of FGF21 in memory formation may be sex-specific (Figures S3P–S3R). These data indicate that pharmacological FGF21 administration does not affect spatial learning, but instead improves short-term and long-term spatial memory formation in healthy lean mice. To assess the role of pharmacological FGF21 in additional types of memory, wild-type mice were subjected to contextual and cued-fear conditioning 1 h after IP administration of FGF21 or saline treatment. Mice treated with FGF21 exhibited increased total freezing time relative to mice treated with saline during cued- and contextual-fear recall (Figures S4A and S4B). Together, these data suggest that pharmacological FGF21 contributes to multiple forms of memory.

At the cellular level, spatial memory is thought to be encoded by a process known as LTP within the hippocampus (Abraham et al., 2019; Whitlock et al., 2006). To evaluate the effect of FGF21 on hippocampal LTP, we next measured LTP in hippocampal slices from wild-type mice after bath application of either artificial cerebrospinal fluid (aCSF) or aCSF plus FGF21 (Figures 3M–3P). Consistent with the behavioral effects associated with FGF21 administration (Figures 3I and 3J), bath application of FGF21 significantly prolonged LTP in hippocampal slices from wild-type mice compared with aCSF alone (Figures 3M–3P). These data reveal that FGF21 administration prolongs LTP in the hippocampus and serves as a likely mechanism by which FGF21 prolongs spatial memory.

FGF21 increases neuron activation and Reelin expression in the hippocampus

Given the effect of FGF21 on hippocampal LTP, we next examined whether KLB, the essential co-receptor for FGF21 signaling, is present in the hippocampus. To accomplish this, we labeled KLB-expressing cells with the fluorescent protein tdTomato by either

crossing *Klb*-CRE mice to Ai14-tdTomato reporter mice (Jensen-Cody et al., 2020) or through viral delivery of a PHP.eB-FLEX-tdTomato virus (Chan et al., 2017) to *Klb*-CRE mice (Jensen-Cody et al., 2020) (Figures 4A and 4B). Importantly, the hippocampus exhibited defined and prominent expression of tdTomato in the dentate gyrus, with more modest expression in the CA1 region of the hippocampus, but very sparse expression in other hippocampal regions (Figures 4A–4C). To identify direct central targets of FGF21, we next evaluated regions of the brain that are activated in response to FGF21 administration using cFos staining. Notably, we observed markedly increased cFos reactivity in KLB^+ neurons in the dentate gyrus of the hippocampus in response to FGF21 administration (Figures 4C and 4D). While we observed increased cFos reactivity in the CA1 region of the hippocampus, this was not in KLB^+ cells. These data suggest that FGF21 directly activates KLB^+ cells in the dentate gyrus.

To explore the cellular identity of KLB^+ cells in the hippocampus and the effects of FGF21 administration on these cells, we performed single-cell RNA-seq on KLB^+ cells from *Klb*-CRE; Ai14-tdTomato mice that were administered vehicle, a single injection of FGF21 (1 mg/kg), or three doses of FGF21 (once/day for 3 days). Unsupervised clustering of KLB^+ cells in the hippocampus revealed both neuronal and non-neuronal cell types (11 clusters total, Figure 4E). Differential expression analyses revealed that FGF21 administration significantly enriched transcriptional programs associated with neurogenesis and post-synaptic organization in KLB^+ granule cell neurons of the dentate gyrus relative to vehicle-treated mice (Figures 4F and 4G). In addition, FGF21 administration for both 1 and 3 days enhanced the expression of the neuromodulating extracellular signaling protein Reelin in Cajal-Retzius cells of the hippocampus relative to vehicle-treated mice (Figures 4F and 4H). Interestingly, while Reelin and Cajal-Retzius cells play an important role in hippocampal organization during development, they have also been described to contribute to spatial memory in the adult dentate gyrus through influencing synaptic plasticity (Beffert et al., 2006; Durakoglugil et al., 2021). Together, these data suggest that FGF21 signals to KLB^+ cells in the hippocampus to modulate neurogenesis, synaptic organization, and synaptic plasticity, key processes related to memory formation (Abrous and Wojtowicz, 2015; Neves et al., 2008).

DISCUSSION

The results from this study reveal that FGF21 is not expressed in hypothalamic tanycytes but is instead expressed in select regions of the brain including the RSC and thalamic nuclei. In addition, we find that FGF21 production from RSC neurons does not regulate energy homeostasis in lean mice but instead contributes to encoding of spatial memory. We used multiple methods, including genetic mouse models, immunohistochemistry and *in silico* analysis of single-cell RNA-seq data, to demonstrate that no detectable FGF21 expression is present in tanycytes or the hypothalamus. Importantly, our *Fgf21*-P2A-CRE; Ai14-tdTomato model is a lineage trace model and expresses tdTomato in any cell that has ever expressed CRE recombinase, regardless of cell- or tissue-specific differences in *Fgf21* expression level. Consistent with our results that FGF21 expression is primarily localized to the RSC and the thalamus, a previous study also observed *Fgf21* mRNA expression in the RSC (Makela et al., 2014).

The reasons for the discrepancy between our findings and those from Geller et al. may be due to multiple technical concerns (Geller et al., 2019). First, while Geller et al. measured *Fgf21* mRNA levels by qPCR, their qPCR primers were not intron spanning (both primers were in exon #1 of *Fgf21* mRNA) (Geller et al., 2019), and it is possible that genomic DNA contamination from incomplete DNase treatment after RNA isolation contributed to their results. Additional studies observing FGF21 expression in the hypothalamus also had errors in qPCR primer design and/or validation (Benomar et al., 2016; Yuan et al., 2019). Second, the antibody used to detect FGF21 by immunohistochemistry appears to be non-specific. Using a secondary antibody control and FGF21 knockout mice, we found that the observed signal in wild-type mice using the same antibodies and methods as Geller et al. was also present in our negative controls. This is likely due to non-specific binding of the FGF21 antibody. Regardless of the reason, the signal was observed in both wild-type and FGF21 knockout mice. Notably, signal was also observed in the FGF21 knockout controls in the Geller et al. study (their Figure S1D) (Geller et al., 2019). Third, the *in vivo* differences observed could potentially be explained by several methodological concerns. Importantly, their study failed to use littermate controls, which can have significant impacts on metabolic measures (Parra-Vargas et al., 2020). Instead, mice with two completely different stock numbers were directly ordered from The Jackson Laboratory and used for experimentation (Geller et al., 2019). In addition, levels of circulating or hepatic FGF21 levels were not reported in these studies. Perhaps administration of the AAV-TAT-CRE resulted in altered hepatic FGF21 levels, thereby altering lipid metabolism and energy homeostasis. There are also issues with how the authors analyzed their metabolic cage data. It appears both oxygen consumption and energy expenditure were normalized by body weight or lean mass, methods that are inappropriate for reporting indirect calorimetry data (Corrigan et al., 2020; Tschop et al., 2011). If these data were analyzed using analysis of covariance or generalized linear modeling, any differences between treatment groups could be diminished, supporting our data that central knockdown of FGF21 does not alter energy balance.

An unexpected result from these studies is the discovery that FGF21 is expressed in the RSC, and RSC-derived FGF21 is required for spatial memory formation. Consistent with this, though, studies have implicated FGF21 in contributing to improved cognitive performance under fasting or protein restriction conditions (Ren et al., 2021; Ruhlmann et al., 2016). Interestingly, pharmacologic FGF21 administration robustly enhances spatial memory formation and recall. In addition, our work suggests FGF21 signaling prolongs hippocampal LTP, which is a well-established cellular correlate of memory formation (Lynch, 2004). Notably, we reveal that hippocampal Reelin expression is induced under FGF21 treatment, and FGF21 enhances dentate gyrus granule cell neuron activity and transcriptional programs associated with neurogenesis. Interestingly, these data suggest that FGF21 may influence memory through more than one mechanism, but additional studies are needed to clarify these effects. Multiple studies demonstrate that Reelin increases synaptic plasticity and LTP in the hippocampus (Pujadas et al., 2010; Rogers et al., 2011; Telese et al., 2015; Weeber et al., 2002). Moreover, Reelin is essential for spatial learning and memory in rodents, and interference of Reelin signaling impairs spatial memory (Stranahan et al., 2011). The ability of FGF21 to increase Reelin expression in Cajal-Retzius cells in

dentate gyrus provides an exciting potential molecular mechanism for FGF21's ability to prolong spatial memory.

While it is not immediately clear why FGF21 would be produced from neurons in the RSC to alter memory formation, perhaps FGF21 production in this region compliments FGF21's known role in macronutrient preference (Flippo et al., 2020; Jensen-Cody et al., 2020; von Holstein-Rathlou et al., 2016). That is, perhaps central FGF21 facilitates the organism's ability to effectively recall the location of macronutrient sources while foraging. Consistent with this, selective hippocampal neurons are active at reward locations, suggesting a role for the hippocampus in navigation during foraging behavior (Jarzebowski et al., 2022). Finally, similar to the sex-dependent effects of FGF21 in mediating the metabolic effects of a low-protein diet (Green et al., 2022), we find that pharmacological administration of FGF21 significantly improves memory formation in male but not female mice.

The data presented here indicate that FGF21 is not expressed or produced from tanycytes *in vivo* and that central FGF21 does not regulate energy homeostasis in lean mice. Thus, central production of FGF21 is functionally distinct from peripherally derived FGF21, a paradigm that has been observed for other hormones, including renin-angiotensin (Grobe et al., 2010), GLP-1 (Vrang and Larsen, 2010), and FGF15 (Picard et al., 2021). Importantly, peripheral FGF21 can travel through the blood-brain barrier and signals through the CNS (e.g., hypothalamus) to regulate energy balance (Hsuchou et al., 2007; Jensen-Cody et al., 2020; Xu et al., 2017). Located at the third ventricle, tanycytes are involved in shuttling peripheral factors, including leptin, ghrelin, and insulin, into the mediobasal hypothalamus to elicit their biological functions (Balland et al., 2014; Collden et al., 2015; Duquenne et al., 2021; Porniece Kumar et al., 2021). However, the mechanism of how peripheral FGF21 enters the CNS has not yet been determined. Our study demonstrates that FGF21 is not produced from hypothalamic tanycytes but does not exclude the possibility that peripheral FGF21 may act on, or be transported by, tanycytes in the hypothalamus. Indeed, our previous work (Jensen-Cody et al., 2020), and work in this study, identified that *Klb* is expressed in hypothalamic tanycytes. The clarification of central versus peripheral FGF21 function is important, as it supports the utility in assessing circulating FGF21 levels in humans as a clinical diagnostic readout of metabolic FGF21 action. The potential regulation of FGF21 production and processing in regions such as the RSC and thalamus, as well as potential synaptic mechanisms by which FGF21 elicits its effects on spatial memory, are important areas of future study.

Limitations of the study

Limitations of this study include the inability to reliably determine the level of FGF21 takeout following virus administration in different brain regions in $FGF21^{fl/fl}$ mice. *Fgf21* mRNA levels are very low in the RSC and have been challenging to measure by qPCR (CT 31–34). This issue is not unique to FGF21, as multiple other factors including KLB (Jensen-Cody et al., 2020) and the leptin receptor (Vong et al., 2011; Xu et al., 2018) also have very low expression in the CNS, and have been difficult to determine takeout. Instead, we use fluorescent reporters to demonstrate CRE delivery to specific cells and/or brain regions. Finally, an additional limitation of this study is the potential role of FGF21

in different brain regions besides the RSC in regulating memory formation. While our data indicate a role for RSC-derived FGF21 in regulating memory formation, we cannot exclude a possible role for FGF21 production from the cerebellum, thalamus, or entorhinal cortex in regulating learning and memory.

STAR★METHODS

RESOURCE AVAILABILITY

Lead contact—Further information and requests for resources and reagents should be directed to and will be fulfilled by the lead contact, Matthew J. Potthoff (matthew-potthoff@uiowa.edu).

Materials availability—All unique/stable reagents generated in this study are available from the Lead Contact.

Data and code availability

- Single-cell RNA sequencing data have been deposited at GEO (GSE208083) and are publicly available as of the date of publication. Accession numbers are listed in the key resources table.
- This paper does not report original code.
- Any additional information required to reanalyze the data reported in this paper is available from the lead contact upon request.

EXPERIMENTAL MODEL AND SUBJECT DETAILS

All experiments presented in this study were conducted according to the animal research guidelines from NIH and were approved by the University of Iowa IACUC.

Animals—The following mice utilized in these studies have been previously described (Jackson Labs stock number in parenthesis): C57BL/6J (000664), Ai14-tdTomato (007914) (Madisen et al., 2010), FGF21 knockout (033846) (Potthoff et al., 2009), *Klb*-CRE (Jensen-Cody et al., 2020), and FGF21$^{fl/fl}$ (022361) (Markan et al., 2014). *Fgf21*-P2A-CRE mice were generated by University of Iowa Genomic Editing Facility using CRISPR in C57BL/6 mice to insert a viral 2A oligopeptide and a CRE recombinase gene immediately downstream of the FGF21 stop codon. Proper targeting was confirmed by genomic sequencing and the mice were crossed four generations to C57BL/6J mice prior to use for experiments. All mice were on a C57BL/6J genetic background. All mice were housed in a 12h light-dark cycle with ad libitum access to chow diets (Teklad 2920x) and water unless stated otherwise. Littermates were randomly assigned to experimental groups. Animal ages are reported in figure and supplemental figure legends.

METHOD DETAILS

Viral infection—4–8 week old FGF21$^{fl/fl}$ mice were anesthetized with 2%–3% isoflurane and injected retro-orbitally with PHP.eB or AAV viruses, pEN-N.AAV.hSyn.HI.eGFP-CRE.WPRE.SV40 (Addgene, PHP.eB) or AAV2/PHP.eB.CMV.eGFP (University of

Iowa Viral Vector Core), AAV8.TBG.PI.Cre.rBG (Addgene) or AAV8.TBG.PI.Null.bGH (Addgene). Similarly, *Fgf21*-P2A-CRE and *Klb*-CRE mice were retro-orbitally injected with pAAV-FLEX-tdTomato virus (Addgene, PHP.eB). Following injection, mice were allowed to recover for a minimum of 2 weeks to allow viral spread.

Stereotaxic injection—7–10 week old mice were anesthetized with 2%–3% isoflurane and placed with a heat pad on the stereotaxic frame. Eye ointment was applied. After applying aseptic betadine and 70% alcohol, an incision was made to expose the skull. A craniotomy was made by a micro-driller. A 1 μL Hamilton syringe was slowly moved to the target coordinates. 0.5–1 μL of AAV virus was injected with the speed approximately 0.02 μL/min. Adeno-associated viruses were injected bilaterally into the posterior retrosplenial cortex (AP −2.255; ML ±0.25; DV −1, 0.8, −0.6, −0.4) of the $FGF21^{fl/fl}$ mice.

Two-bottle choice experiments—For two-bottle tastant experiments, drinking tubes were constructed and test fluids were presented following the Monell Mouse Taste Phenotyping Project specifications (http://www.monell.org/MMTPP/), and mice were offered the indicated amount of sucrose versus water. Animals were individually caged with ad libitum chow. Solutions were available 23h/day and sucrose intake was recorded and tubes were refilled during the remaining hour. For two-bottle choice experiments, all solutions were prepared with tap water and served at room temperature. The experiment lasted for 7 days consisting of first 2 days for acclimation, and the next 5 days during which, mice preference for sucrose versus water reached a plateau. For sucrose intake studies, mice were randomly assigned to groups and mice that were unwilling to drink were removed from analysis.

Metabolic cage studies—$FGF21^{fl/fl}$ mice were individually housed in the Promethion Metabolic System (Sable Systems International) at the University of Iowa Metabolic Phenotyping Core on a 12h light-dark cycle with ad libitum access to water and food. Cages were mounted inside thermally controlled cabinets maintained at 30°C. Each cage was connected to a flow regulator and gas analyzer to measure oxygen consumption and carbon dioxide production. Food intake was measured manually in home cages.

Plasma assay—Trunk blood was collected into 300K2E microvettes (Sarstedt) and spun at 3000 rpm for 30 min at 4°C to separate plasma. Plasma triglycerides (Infinity, Thermo Scientific), β-hydroxybutyrate (Wako Diagnostics), NEFA (Wako Diagnostics) and glucose (Wako Diagnostics) were measured using colorimetric assays. All measurements were performed according to the manufacturer's instructions.

Barnes maze—The Barnes Maze (Patil et al., 2009) was conducted on a gray circular surface 91 cm in diameter, with 20 holes 5 cm in diameter equally spaced around the perimeter (Noldus). An escape chamber was randomly placed underneath the same hole for the duration of the training. The maze was surrounded by a white curtain with four different visual cues for orientation to the location of the escape chamber and a bright light was placed above the maze to motivate the animal to find the dark escape chamber. Each animal was subjected to four days of training comprising of four trials per day. If the mouse did not

find the escape chamber within 3 min, they were gently led to the hole containing the escape chamber.

For the experiment of the $FGF21^{fl/fl}$ mice administered the PHP.eB or TBG viruses, the same mice were used for both the metabolic cage and Barnes Maze experiments. The metabolic cages experiments were performed first and then mice were provided one week of rest before initiating the Barnes Maze training. The probe trial for these groups of mice were performed 24 h after training, during which the escape chamber was removed. For the experiment of C57BL/6J mice administered FGF21, a probe trial was conducted on the 24 h, day 7, day 21, day 28, and day 35 after the training, during which the escape chamber was removed. Similarly, a probe trial was conducted on the 24h, day 7, and day 14 after the training for the experiment of $FGF21^{fl/fl}$ mice that received AAV-CRE viruses in the RSC. Measurements were made to evaluate the animal's short and long-term memory based on spatial cues. Measurements were acquired with Ethovision XT 11.5 video tracking software (Noldus) and confirmed by tracking the videos manually. Recombinant FGF21 was generated and provided by Novo Nordisk. For Barnes Maze studies, mice were administered i.p. injections of vehicle or FGF21 at 1 mg/kg, and the training was initiated 1 h after the drug treatment.

Fear conditioning—Contextual and cued-fear conditioning was done as described (Sowers et al., 2013), using a near-infrared video-equipped fear conditioning chamber (Med Associates, Inc.). Freezing was scored with VideoFreeze software (Med Associates, Inc.). On day 1, context and cued-fear training was performed for 14 min. Mice were allowed to explore the chamber for 3 min, and then 5 tones (80 dB, 3 kHz, 20 s) followed by a shock (1 s, 0.75 mA) were delivered with an inter-trial interval of 100s. To test conditioned freezing to the tone, on day 2, mice were placed in a different context (a smooth white floor and a triangle insert were placed in the chamber with peppermint spray to change the odor of the environment). Freezing was scored over 10 min, with the tone occurring during 3–6 min. On day 3, mice were placed back to the day 1 conditioning chamber for 6 min without foot shocks to test the contextual-fear memory. Freezing was scored with VideoFreeze software.

Immunohistochemistry—Immunohistochemistry was performed as previously described (Geller et al., 2019). Mice were transcardially perfused with saline followed by 4% paraformaldehyde. Brains were collected and stored in 4% PFA overnight followed by 30% sucrose for 48 h. Coronal brain sections (50 μm) were collected using a cryostat (Leica). Free-floating sections were washed in 1X PBS and incubated in Citrate Buffer (Abcam) for 15 min at room temperature (RT), followed by 2 min at 60 C° and 90 C°. Slices were incubated in blocking buffer (5% donkey serum in PBST) for 1 h at RT and incubated in primary rabbit monoclonal anti-Fgf21 (1:100, Abcam) for three nights and chicken anti-Vimentin (1:2000, Millipore) overnight at 4 C°. Sections were subsequently washed and incubated in secondary antibody donkey anti-rabbit AF594 and donkey anti-chicken AF647 (Jackson Immunoresearch) or goat anti-rabbit Texas Red and goat anti-chicken AF488 for 2 h at RT. Slices were mounted on slides with Vectashield antifade mounting media with DAPI and imaged using an Olympus BX61 Light Microscope or an Olympus FV3000 confocal

laser scanning microscope. Staining for cFos was performed as previously using a cFos antibody (1:1000, Cell Signaling) (Jensen-Cody et al., 2020).

***In situ* hybridization—**Mice were euthanized and brain tissue was collected, frozen in 2-methylbutane, embedded into medium (Tissue-Tek O.C.T. Compound) and stored at −80°C. 10-μm coronal sections were cut using a cryostat and stored at −80°C until use. Tissue sections underwent treatment and hybridization according to manufacturer (Advanced Cell Diagnostics) instructions for fresh frozen tissue (Multiplex Fluorescent Reagent Kit v2 User Manual). Briefly, slides were transferred from −80°C directly into 4% paraformaldehyde at 4°C. Slides were rinsed and dehydrated in increasing ethanol concentrations before treatment with hydrogen peroxide and pro-tease IV at room temperature. Slides were subsequently moved to 40°C (HybEZ oven; ACD) for hybridization with probes targeting FGF21 (460931) and tdTomato (317041-C2), as well as positive (Mm-Ppib; 313911) and negative (DapB; 310043) control probes. The hybridization signal was amplified, developed, and subsequently incubated with fluorescent probes Opal 520 and Opal 570 (Akoya Biosciences). After every incubation step, slides were washed in 1X Wash Buffer three times (2 min each). Slides were coverslipped with mounting media (VECTASHIELD) and imaged with a Leica STED.

Gene expression—Gene expression analysis were performed as described (BonDurant et al., 2017). RNA was isolated from total liver, retrosplenial cortex, or hypothalamus following Trizol (Invitrogen) protocol. 2 micrograms RNA from each sample was used to generate cDNA (High-Capacity cDNA Reverse Transcription Kit; Life Technologies), and QPCR was conducted using SYBR green (Invitrogen). QPCR primers sequences are as follows: mU36B4: 5′-CGTCCTCGTTGGAGTGACA-3′, 5′-CGGTGCGTCAGGGATTG-3′; FGF21: 5′-CCTCTAGGTTT CTTTGCCAACAG-3′, 5′-AAGCTGCAGGCCTCAGGAT-3′; CRE: 5′-TGTTGCCGCGCCATCTG-3′, 5′-TTGCTTCAAAAATCCCTTCCA-3′.

***In silico* analysis of deposited single-cell RNA sequencing—**Single cell RNA sequencing data of the whole hypothalamus (Campbell et al., 2017; Chen et al., 2017) and thalamus (Saunders et al., 2018) was downloaded from the Broad Single Cell Portal (Campbell et al., 2017), GEO, accession number: GSE87544 (Chen et al., 2017), and dropviz.org (Saunders et al., 2018) and loaded into the R package Seurat (v3.1). Within the datasets representing the hypothalamus cells identified as tanycytes were extracted and in the thalamic dataset only cells which expressed *Fgf21* were extracted due to the large size of the dataset. The three datasets were then integrated using the Seurat to compare FGF21 expression, among other genes, across tanycytes and thalamic cells expressing FGF21. In total this dataset represents more than 5,000 cells. Additional analysis for supplementary figures was carried out using the whole dataset from a recent paper looking at developmental gene expression at the single cell level in the hypothalamus ((Romanov et al., 2020), GEO: GSE132730). In this dataset only a single cell (out of more than 50,000 sequenced) was found to express *Fgf21* which was classified as a neuron.

Hippocampal slice preparation—Acute hippocampal slices were prepared as previously described (Shetty et al., 2015). All reagents were purchased from Sigma (St. Louis, MO). Briefly, the hippocampus was quickly dissected out of the brain in ice-cold aCSF (124 mM NaCl, 4.4 mM KCl, 1 mM NaH_2PO_4, 2.5 mM $CaCl_2.2H_2O$, 1.3 mM $MgSO_4.7H_2O$, 26.2 mM $NaHCO_3$, and 10 mM D-glucose) saturated with carbogen. 400 μm thick transverse hippocampal slices were prepared using a tissue slicer (Stoelting, Wooddale, IL) and slices were immediately transferred into cold aCSF bubbled continuously with carbogen (95% O_2 and 5% CO_2). Slices were then transferred to a humidified interface chamber (Fine Science Tools, Foster City, CA) continuously perfused with aCSF saturated with carbogen at a flow rate of 1mL/min and allowed to recover at 30 C for at least 2h.

Extracellular recordings—Extracellular recordings were performed using aCSF filled glass microelectrodes (1–5MΩ resistance) pulled from borosilicate glass (BF150-110-10, Sutter Instruments, CA) using a pipette puller (P1000, Sutter Instruments, CA). Lacquer coated stainless steel monopolar electrodes (#571000, A-M Systems, Colorado Springs, CO) were used for stimulation. Stimulation of CA3 projections (schaffer-collateral pathway) and recording of synapses was performed within stratum radiatum of area CA1. Biphasic constant current pulses generated by an isolated pulse stimulator (Model 2100, A-M systems, Colorado Springs, CO) was used to stimulate the schaffer-collaterals and synaptic responses were recorded using an intracellular electrometer (IE-251A, Warner Instruments, MA). Amplified signals were filtered at 2kHz using a low-pass bessel filter (LPF 100B, Warner Instruments, MA). Filtered signals were digitized (Digidata 1440, Axon Instruments, CA) and acquired at 20kHz using pCLAMP 11 (Molecular Devices, Union City, CA). Baseline recordings were performed with stimulation intensity that elicited 30–40% of maximal fEPSP amplitudes for 60 min and test pulses were delivered at 0.016 Hz before a single tetanic stimulation (100Hz, 1s; pulse width- 0.1ms per half-wave) was delivered to induce E-LTP. For FGF21 treatment, after 20 min of baseline recording, slices were perfused with FGF21 (50 μg/mL in aCSF) for 40 min prior to a single tetanic stimulation followed by another 20 min perfusion with aCSF containing FGF21 (50μg/mL). Data were extracted using Clampfit 11.2 software (Molecular Devices, Union City, CA) and fEPSP slopes (20%–80%) were measured. The average of fEPSP slopes from the first 20 min of baseline recording was used to normalize the data and “n” refers to slices.

Tissue clearing, imaging, and processing—An augmented DISCO protocol was utilized to clear whole brain tissue of *Fgf21*-P2A-CRE; Ai14-tdTomato and CRE negative control mice as previously described (Claflin et al., 2022). Mice were anesthetized and transcardially perfused with pH 9.5 saline followed by pH 9.5 4% PFA. After post-fixing in PFA overnight, the brains were washed 3 times in saline and dehydrated with 50% tetrahydrofuran (THF) in dH_2O for 24 h. Every 24 h the brains were transferred to a higher concentration of THF (50%, 70%, 80%), all at pH = 9.5. Brains were incubated in 100% THF for 48 h, and the solution was replaced every 12 h to maximize tissue THF concentration. After the final incubation in 100% THF, brains were transferred to dichloromethane (DCM) for 3 h followed by BABB-D15 for 4 h, as previously (Pan et al., 2016). All steps were performed at 4°C in the dark. Additionally, after transferring brains to a new solution, argon gas was flowed over the sample to minimize oxygen interaction

with the sample. Cleared brains were imaged in BABB-D15 using a light sheet fluorescence microscope (LaVision BioTec Ultramicroscope II) interfaced with an Andor *Neo* sCMOS camera, an Olympus MVX10 zoom microscope body, and a MVPLAPO 2x dipping cap. Whole brain three-dimensional images were achieved using a 3×3 mosaic tile scan of a 2x optical zoom and a z stack with step size of 2.5 μm. The raw lossless TIFF files of the collected tile scans were stitched using the ImspectorPro software and reconstructed into three dimensions with Imaris File Converter. Images and movies of brain samples were captured with Imaris.

Generation of single cell suspensions—The method used here for generating single cell suspensions was modified from a previously published protocol32. Individual mice were quickly decapitated, the brain was immediately extracted and placed in fresh ice-cold artificial cerebrospinal fluid (aCSF) containing 124 mM NaCl, 2.5 mM KCl, 1.2 mM NaH2PO4, 24 mM NaHCO3, 5 mM HEPES, 13 mM glucose, 2 mM MgSO4, and 2 mM CaCl2, bubbled with a carbogen gas (95% O2 and 5% CO2) and with a pH of 7.3–7.4. Brains were then sectioned on a vibratome and sections containing the dorsal hippocampus were placed in ice-cold aCSF w/actinomycin D (93 mM N-methyl-D-glucamine, 2.5 mM KCl, 1.2 mM NaH2PO4, 30 mM NaHCO3, 20 mM HEPES, 25 mM glucose, 10 mM MgSO4, 0.5 mM CaCl2, 5 mM sodium ascorbate, 2 mM thiourea, and 3 mM sodium pyruvate, 45 μM actinomycin D, pH of 7.3–7.4, bubbled with carbogen gas (95% O2 and 5% CO2) on ice for at least 15 min prior to dissection). The dorsal hippocampus was then dissected from each section, and tissue derived from three mice were pooled for each experimental condition. The tissue was then minced and placed in 2mg/ml Pronase in aCSF w/actinomycin D and incubated at 37°C for 30 min. Following digestion, the Pronase solution was exchanged with ice-cold, carbogen-bubbled ACSF containing 1% fetal bovine serum and .01% BSA. The tissue was then titrurated using fire polished Pasteur pipets and strained through a 70 μM cell strainer.

FACS sorting—FACs sorting for tdTomato positive cells was performed as previously described21. Hoechst cell viability dye (Hoechst 33258) was added to the cell suspension at a final dilution of 4ug/ml just prior to sorting to allow for selection of living cells during FACs sorting. Cells were then FACs sorted for tdTomato fluorescence and viability via Hoechst staining. Sorting was performed on a BD FACS Aria II using a 130 mM nozzle, a sheath pressure of 10 p.s.i., and in the single cell sorting mode at the University of Iowa Flow Cytometry Facility.

Single cell capture and cDNA library construction—FACS isolated cells were then loaded on the BD Rhapsody where capture of the single cells was performed per manufacturer instructions. Following lysis of the cells and capture of mRNA on oligonucleotide barcoded beads the cDNA synthesis was performed and cDNA libraries with Illumina sequencing adapters were generated per manufacturer instructions using the BD Rhapsody whole transcriptome analysis amplification kit. cDNA libraries were then sequenced on Illumina NovaSeq 6000 sequencers at the University of Iowa Genomics Core. Sequencing data was then quality filtered and annotated using the BD Rhapsody analysis pipeline while also correcting for artifacts which arise during library construction.

Filtered and annotated data from vehicle and FGF21 treated mice were then normalized in the R package Seurat. Imputation was performed using the Seurat Wrapper ALRA on the normalized dataset before final clustering (clustering resolution was set at 0.5 based on the number of cells sequenced) and gene expression analysis to account for dropout associated with 3′-barcoding-based approaches. “Cell type” classification of the clusters was determined based on expression of previously identified marker genes (mousebrain.org) for neuronal and non-neuronal cell types.

QUANTIFICATION AND STATISTICAL ANALYSIS

Data analysis was performed using GraphPad Prism software (GraphPad Inc., San Diego, CA, USA) and presented as mean ± SEM; $p < 0.05$ was considered significant. “n” represents to the number of individual mice used in each experiment. The statistical test used for each comparison is described in the corresponding figure legends.

Supplementary Material

Refer to Web version on PubMed Central for supplementary material.

ACKNOWLEDGMENTS

We thank Dr. Birgitte Andersen (Novo Nordisk) for providing FGF21 protein. This work was funded by the National Institutes of Health (NIH) R01DK106104 (M.J.P.), R01AA027654 (M.J.P.), F32 DK117510 (K.E.C.), T32 DK112751 (K.H.F.), R01 MH117964 to (T.A.), The University of Iowa Hawkeye Intellectual and Developmental Disabilities Research Center (HAWK-IDDRC) P50 HD103556 (T.A.), and the Veterans Affairs Merit Review Program I01BX004634 (M.J.P.). M.J.P. and T.A. are also supported by the Roy J. Carver Charitable Trust. The authors thank Dr. Mahesh Shivarama Shetty for assistance with electrophysiology and for feedback on the manuscript. The authors also acknowledge the use of the University of Iowa Central Microscopy Research Facility, which is supported by the University of Iowa Vice President for Research and/or the Carver College of Medicine.

REFERENCES

Abraham WC, Jones OD, and Glanzman DL (2019). Is plasticity of synapses the mechanism of long-term memory storage? NPJ Sci. Learn 4, 9. 10.1038/s41539-019-0048-y. [PubMed: 31285847]

Abrous DN, and Wojtowicz JM (2015). Interaction between neurogenesis and hippocampal memory system: new vistas. Cold Spring Harb. Perspect. Biol 7, a018952. 10.1101/cshperspect.a018952.

Adams AC, Cheng CC, Coskun T, and Kharitonenkov A (2012). FGF21 requires betaklotho to act in vivo. PLoS One 7, e49977. 10.1371/journal.pone.0049977.

Ameka M, Markan KR, Morgan DA, BonDurant LD, Idiga SO, Naber MC, Zhu Z, Zingman LV, Grobe JL, Rahmouni K, and Potthoff MJ (2019). Liver derived FGF21 maintains Core body temperature during acute cold exposure. Sci. Rep 9, 630. 10.1038/s41598-018-37198-y. [PubMed: 30679672]

Balland E, Dam J, Langlet F, Caron E, Steculorum S, Messina A, Rasika S, Falluel-Morel A, Anouar Y, Dehouck B, et al. (2014). Hypothalamic tanycytes are an ERK-gated conduit for leptin into the brain. Cell Metab. 19, 293–301. 10.1016/j.cmet.2013.12.015. [PubMed: 24506870]

Beffert U, Durudas A, Weeber EJ, Stolt PC, Giehl KM, Sweatt JD, Hammer RE, and Herz J (2006). Functional dissection of Reelin signaling by site-directed disruption of Disabled-1 adaptor binding to apolipoprotein E receptor 2: distinct roles in development and synaptic plasticity. J. Neurosci 26, 2041–2052. 10.1523/JNEUROSCI.4566-05.2006. [PubMed: 16481437]

Benomar Y, Amine H, Crépin D, Al Rifai S, Riffault L, Gertler A, and Taouis M (2016). Central Resistin/TLR4 impairs adiponectin signaling, contributing to insulin and FGF21 resistance. Diabetes 65, 913–926. 10.2337/db15-1029. [PubMed: 26740596]

BonDurant LD, Ameka M, Naber MC, Markan KR, Idiga SO, Acevedo MR, Walsh SA, Ornitz DM, and Potthoff MJ (2017). FGF21 regulates metabolism through adipose-dependent and -independent mechanisms. Cell Metab. 25, 935–944.e4. 10.1016/j.cmet.2017.03.005. [PubMed: 28380381]

BonDurant LD, and Potthoff MJ (2018). Fibroblast growth factor 21: a versatile regulator of metabolic homeostasis. Annu. Rev. Nutr 38, 173–196. 10.1146/annurev-nutr-071816-064800. [PubMed: 29727594]

Campbell JN, Macosko EZ, Fenselau H, Pers TH, Lyubetskaya A, Tenen D, Goldman M, Verstegen AMJ, Resch JM, McCarroll SA, et al. (2017). A molecular census of arcuate hypothalamus and median eminence cell types. Nat. Neurosci 20, 484–496. 10.1038/nn.4495. [PubMed: 28166221]

Chan KY, Jang MJ, Yoo BB, Greenbaum A, Ravi N, Wu WL, Sánchez-Guardado L, Lois C, Mazmanian SK, Deverman BE, and Gradinaru V (2017). Engineered AAVs for efficient noninvasive gene delivery to the central and peripheral nervous systems. Nat. Neurosci 20, 1172–1179. 10.1038/nn.4593. [PubMed: 28671695]

Chen R, Wu X, Jiang L, and Zhang Y (2017). Single-cell RNA-seq reveals hypothalamic cell Diversity. Cell Rep. 18, 3227–3241. 10.1016/j.celrep.2017.03.004. [PubMed: 28355573]

Claflin KE, Flippo KH, Sullivan AI, Naber MC, Zhou B, Neff TJ, Jensen-Cody SO, and Potthoff MJ (2022). Conditional gene targeting using UCP1-Cre mice directly targets the central nervous system beyond thermogenic adipose tissues. Mol. Metab 55, 101405. 10.1016/j.molmet.2021.101405.

Collden G, Balland E, Parkash J, Caron E, Langlet F, Prevot V, and Bouret SG (2015). Neonatal overnutrition causes early alterations in the central response to peripheral ghrelin. Mol. Metab 4, 15–24. 10.1016/j.molmet.2014.10.003. [PubMed: 25685686]

Corrigan JK, Ramachandran D, He Y, Palmer CJ, Jurczak MJ, Chen R, Li B, Friedline RH, Kim JK, Ramsey JJ, et al. (2020). A big-data approach to understanding metabolic rate and response to obesity in laboratory mice. Elife 9, e53560. 10.7554/eLife.53560.

Czajkowski R, Jayaprakash B, Wiltgen B, Rogerson T, Guzman-Karlsson MC, Barth AL, Trachtenberg JT, and Silva AJ (2014). Encoding and storage of spatial information in the retrosplenial cortex. Proc. Natl. Acad. Sci. USA 111, 8661–8666. 10.1073/pnas.1313222111. [PubMed: 24912150]

Ding X, Boney-Montoya J, Owen BM, Bookout AL, Coate KC, Mangelsdorf DJ, and Kliewer SA (2012). betaKlotho is required for fibroblast growth factor 21 effects on growth and metabolism. Cell Metab. 16, 387–393. 10.1016/j.cmet.2012.08.002. [PubMed: 22958921]

Duquenne M, Folgueira C, Bourouh C, Millet M, Silva A, Clasadonte J, Imbernon M, Fernandois D, Martinez-Corral I, Kusumakshi S, et al. (2021). Leptin brain entry via a tanycytic LepR-EGFR shuttle controls lipid metabolism and pancreas function. Nat. Metab 3, 1071–1090. 10.1038/s42255-021-00432-5. [PubMed: 34341568]

Durakoglugil MS, Wasser CR, Wong CH, Pohlkamp T, Xian X, Lane-Donovan C, Fritschle K, Naestle L, and Herz J (2021). Reelin regulates neuronal Excitability through striatal-enriched protein tyrosine phosphatase (STEP61) and calcium permeable AMPARs in an NMDAR-dependent manner. J. Neurosci 41, 7340–7349. 10.1523/JNEUROSCI.0388-21.2021. [PubMed: 34290083]

Fisher FM, and Maratos-Flier E (2016). Understanding the physiology of FGF21. Annu. Rev. Physiol 78, 223–241. 10.1146/annurev-physiol-021115-105339. [PubMed: 26654352]

Flippo KH, Jensen-Cody SO, Claflin KE, and Potthoff MJ (2020). FGF21 signaling in glutamatergic neurons is required for weight loss associated with dietary protein dilution. Sci. Rep 10, 19521. 10.1038/s41598-020-76593-2.

Flippo KH, and Potthoff MJ (2021). Metabolic messengers: FGF21. Nat. Metab 3, 309–317. 10.1038/s42255-021-00354-2. [PubMed: 33758421]

Flippo KH, Trammell SAJ, Gillum MP, Aklan I, Perez MB, Yavuz Y, Smith NK, Jensen-Cody SO, Zhou B, Claflin KE, et al. (2022). FGF21 suppresses alcohol consumption through an amygdalo-striatal circuit. Cell Metab. 34, 317–328.e6. 10.1016/j.cmet.2021.12.024. [PubMed: 35108517]

Fon Tacer K, Bookout AL, Ding X, Kurosu H, John GB, Wang L, Goetz R, Mohammadi M, Kuro-o M, Mangelsdorf DJ, and Kliewer SA (2010). Research resource: comprehensive expression atlas of the fibroblast growth factor system in adult mouse. Mol. Endocrinol 24, 2050–2064. 10.1210/me.2010-0142. [PubMed: 20667984]

Geller S, Arribat Y, Netzahualcoyotzi C, Lagarrigue S, Carneiro L, Zhang L, Amati F, Lopez-Mejia IC, and Pellerin L (2019). Tanycytes regulate lipid homeostasis by sensing free fatty acids and signaling to key hypothalamic neuronal populations via FGF21 secretion. Cell Metab. 30, 833–844.e7. 10.1016/j.cmet.2019.08.004. [PubMed: 31474567]

Green CL, Pak HH, Richardson NE, Flores V, Yu D, Tomasiewicz JL, Dumas SN, Kredell K, Fan JW, Kirsh C, et al. (2022). Sex and genetic background define the metabolic, physiologic, and molecular response to protein restriction. Cell Metab. 34, 209–226.e5. 10.1016/j.cmet.2021.12.018. [PubMed: 35108511]

Grobe JL, Grobe CL, Beltz TG, Westphal SG, Morgan DA, Xu D, de Lange WJ, Li H, Sakai K, Thedens DR, et al. (2010). The brain Reninangiotensin system controls divergent efferent mechanisms to regulate fluid and energy balance. Cell Metab. 12, 431–442. 10.1016/j.cmet.2010.09.011. [PubMed: 21035755]

Harno E, Cottrell EC, and White A (2013). Metabolic pitfalls of CNS Cre-based technology. Cell Metab. 18, 21–28. 10.1016/j.cmet.2013.05.019. [PubMed: 23823475]

Hsuchou H, Pan W, and Kastin AJ (2007). The fasting polypeptide FGF21 can enter brain from blood. Peptides 28, 2382–2386. 10.1016/j.peptides.2007.10.007. [PubMed: 17996984]

Jarzebowski P, Hay YA, Grewe BF, and Paulsen O (2022). Different encoding of reward location in dorsal and intermediate hippocampus. Curr Biol. 32, 834–841.e5. 10.1016/j.cub.2021.12.024. [PubMed: 35016008]

Jensen-Cody SO, Flippo KH, Claflin KE, Yavuz Y, Sapouckey SA, Walters GC, Usachev YM, Atasoy D, Gillum MP, and Potthoff MJ (2020). FGF21 signals to glutamatergic neurons in the ventromedial hypothalamus to suppress carbohydrate intake. Cell Metab. 32, 273–286.e6. 10.1016/j.cmet.2020.06.008. [PubMed: 32640184]

Kurosu H, Choi M, Ogawa Y, Dickson AS, Goetz R, Eliseenkova AV, Mohammadi M, Rosenblatt KP, Kliewer SA, and Kuro-O M (2007). Tissue-specific expression of betaKlotho and fibroblast growth factor (FGF) receptor isoforms determines metabolic activity of FGF19 and FGF21. J. Biol. Chem 282, 26687–26695. 10.1074/jbc.M704165200. [PubMed: 17623664]

Lynch MA (2004). Long-term potentiation and memory. Physiol. Rev 84, 87–136. 10.1152/physrev.00014.2003. [PubMed: 14715912]

Madisen L, Zwingman TA, Sunkin SM, Oh SW, Zariwala HA, Gu H, Ng LL, Palmiter RD, Hawrylycz MJ, Jones AR, et al. (2010). A robust and high-throughput Cre reporting and characterization system for the whole mouse brain. Nat. Neurosci 13, 133–140. 10.1038/nn.2467. [PubMed: 20023653]

Makela J, Tselykh TV, Maiorana F, Eriksson O, Do HT, Mudo G, Korhonen LT, Belluardo N, and Lindholm D (2014). Fibroblast growth factor-21 enhances mitochondrial functions and increases the activity of PGC-1alpha in human dopaminergic neurons via Sirtuin-1. SpringerPlus 3, 2. 10.1186/2193-1801-3-2. [PubMed: 25932355]

Markan KR, Naber MC, Ameka MK, Anderegg MD, Mangelsdorf DJ, Kliewer SA, Mohammadi M, and Potthoff MJ (2014). Circulating FGF21 is liver derived and enhances glucose uptake during refeeding and overfeeding. Diabetes 63, 4057–4063. 10.2337/db14-0595. [PubMed: 25008183]

Mina AI, LeClair RA, LeClair KB, Cohen DE, Lantier L, and Banks AS (2018). CalR: a web-based analysis tool for indirect calorimetry experiments. Cell Metab. 28, 656–666.e1. 10.1016/j.cmet.2018.06.019. [PubMed: 30017358]

Neves G, Cooke SF, and Bliss TVP (2008). Synaptic plasticity, memory and the hippocampus: a neural network approach to causality. Nat. Rev. Neurosci 9, 65–75. 10.1038/nrn2303. [PubMed: 18094707]

Owen BM, Ding X, Morgan DA, Coate KC, Bookout AL, Rahmouni K, Kliewer SA, and Mangelsdorf DJ (2014). FGF21 acts centrally to induce sympathetic nerve activity, energy expenditure, and weight loss. Cell Metab. 20, 670–677. 10.1016/j.cmet.2014.07.012. [PubMed: 25130400]

Owen BM, Mangelsdorf DJ, and Kliewer SA (2015). Tissue-specific actions of the metabolic hormones FGF15/19 and FGF21. Trends Endocrinol. Metab 26, 22–29. 10.1016/j.tem.2014.10.002. [PubMed: 25476453]

Pan C, Cai R, Quacquarelli FP, Ghasemigharagoz A, Lourbopoulos A, Matryba P, Plesnila N, Dichgans M, Hellal F, and Ertürk A (2016). Shrinkage-mediated imaging of entire organs and organisms using uDISCO. Nat. Methods 13, 859–867. 10.1038/nmeth.3964. [PubMed: 27548807]

Parra-Vargas M, Ramon-Krauel M, Lerin C, and Jimenez-Chillaron JC (2020). size does matter: Litter size strongly determines adult metabolism in rodents. Cell Metabol. 32, 334–340.

Patil SS, Sunyer B, Höger H, and Lubec G (2009). Evaluation of spatial memory of C57BL/6J and CD1 mice in the Barnes maze, the Multiple T-maze and in the Morris water maze. Behav. Brain Res 198, 58–68. 10.1016/j.bbr.2008.10.029. [PubMed: 19022298]

Picard A, Metref S, Tarussio D, Dolci W, Berney X, Croizier S, Labouebe G, and Thorens B (2021). Fgf15 neurons of the Dorsomedial hypothalamus control glucagon secretion and hepatic gluconeogenesis. Diabetes 70, 1443–1457. 10.2337/db20-1121. [PubMed: 33883213]

Porniece Kumar M, Cremer AL, Klemm P, Steuernagel L, Sundaram S, Jais A, Hausen AC, Tao J, Secher A, Pedersen TÅ, et al. (2021). Insulin signalling in tanycytes gates hypothalamic insulin uptake and regulation of AgRP neuron activity. Nat. Metab 3, 1662–1679. 10.1038/s42255-021-00499-0. [PubMed: 34931084]

Potthoff MJ, Inagaki T, Satapati S, Ding X, He T, Goetz R, Mohammadi M, Finck BN, Mangelsdorf DJ, Kliewer SA, and Burgess SC (2009). FGF21 induces PGC-1alpha and regulates carbohydrate and fatty acid metabolism during the adaptive starvation response. Proc. Natl. Acad. Sci. USA 106, 10853–10858. 10.1073/pnas.0904187106. [PubMed: 19541642]

Pujadas L, Gruart A, Bosch C, Delgado L, Teixeira CM, Rossi D, de Lecea L, Martínez A, Delgado-García JM, and Soriano E (2010). Reelin regulates postnatal neurogenesis and enhances spine hypertrophy and long-term potentiation. J. Neurosci 30, 4636–4649. 10.1523/jneurosci.5284-09.2010. [PubMed: 20357114]

Ren B, Wang L, Shi L, Jin X, Liu Y, Liu RH, Yin F, Cadenas E, Dai X, Liu Z, and Liu X (2021). Methionine restriction alleviates age-associated cognitive decline via fibroblast growth factor 21. Redox Biol. 41, 101940. 10.1016/j.redox.2021.101940.

Rogers JT, Rusiana I, Trotter J, Zhao L, Donaldson E, Pak DTS, Babus LW, Peters M, Banko JL, Chavis P, et al. (2011). Reelin supplementation enhances cognitive ability, synaptic plasticity, and dendritic spine density. Learn. Mem 18, 558–564. 10.1101/lm.2153511. [PubMed: 21852430]

Romanov RA, Tretiakov EO, Kastriti ME, Zupancic M, Häring M, Korchynska S, Popadin K, Benevento M, Rebernik P, Lallemend F, et al. (2020). Molecular design of hypothalamus development. Nature 582, 246–252. 10.1038/s41586-020-2266-0. [PubMed: 32499648]

Rühlmann C, Wölk T, Blümel T, Stahn L, Vollmar B, and Kuhla A (2016). Long-term caloric restriction in ApoE-deficient mice results in neuroprotection via Fgf21-induced AMPK/mTOR pathway. Aging (Albany NY) 8, 2777–2789. 10.18632/aging.101086. [PubMed: 27902456]

Saunders A, Macosko EZ, Wysoker A, Goldman M, Krienen FM, de Rivera H, Bien E, Baum M, Bortolin L, Wang S, et al. (2018). Molecular Diversity and specializations among the cells of the adult mouse brain. Cell 174, 1015–1030.e16. 10.1016/j.cell.2018.07.028. [PubMed: 30096299]

Shetty MS, Sharma M, Hui NS, Dasgupta A, Gopinadhan S, and Saji-kumar S (2015). Investigation of synaptic tagging/capture and cross-capture using acute hippocampal slices from rodents. J Vis Exp, 53008. 10.3791/53008.

Sostre-Colón J, Gavin MJ, Santoleri D, and Titchenell PM (2022). Acute deletion of the FOXO1-dependent Hepatokine FGF21 does not alter basal glucose homeostasis or lipolysis in mice. Endocrinology 163, 10. 10.1210/endocr/bqac035.

Sowers LP, Loo L, Wu Y, Campbell E, Ulrich JD, Wu S, Paemka L, Wassink T, Meyer K, Bing X, et al. (2013). Disruption of the non-canonical Wnt gene PRICKLE2 leads to autism-like behaviors with evidence for hippocampal synaptic dysfunction. Mol. Psychiatry 18, 1077–1089. 10.1038/mp.2013.71. [PubMed: 23711981]

Stranahan AM, Salas-Vega S, Jiam NT, and Gallagher M (2011). Interference with reelin signaling in the lateral entorhinal cortex impairs spatial memory. Neurobiol. Learn. Mem 96, 150–155. 10.1016/j.nlm.2011.03.009. [PubMed: 21492744]

Telese F, Ma Q, Perez PM, Notani D, Oh S, Li W, Comoletti D, Ohgi KA, Taylor H, and Rosenfeld MG (2015). LRP8-Reelin-Regulated neuronal enhancer signature underlying learning and memory formation. Neuron 86, 696–710. 10.1016/j.neuron.2015.03.033. [PubMed: 25892301]

Todd TP, Fournier DI, and Bucci DJ (2019). Retrosplenial cortex and its role in cue-specific learning and memory. Neurosci. Biobehav. Rev 107, 713–728. 10.1016/j.neubiorev.2019.04.016. [PubMed: 31055014]

Tschöp MH, Speakman JR, Arch JRS, Auwerx J, Brüning JC, Chan L, Eckel RH, Farese RV Jr., Galgani JE, Hambly C, et al. (2011). A guide to analysis of mouse energy metabolism. Nat. Methods 9, 57–63. 10.1038/nmeth.1806. [PubMed: 22205519]

von Holstein-Rathlou S, BonDurant LD, Peltekian L, Naber MC, Yin TC, Claflin KE, Urizar AI, Madsen AN, Ratner C, Holst B, et al. (2016). FGF21 mediates endocrine control of simple sugar intake and sweet taste preference by the liver. Cell Metab. 23, 335–343. 10.1016/j.cmet.2015.12.003. [PubMed: 26724858]

Vong L, Ye C, Yang Z, Choi B, Chua S Jr., and Lowell BB (2011). Leptin action on GABAergic neurons prevents obesity and reduces inhibitory tone to POMC neurons. Neuron 71, 142–154. 10.1016/j.neuron.2011.05.028. [PubMed: 21745644]

Vrang N, and Larsen PJ (2010). Preproglucagon derived peptides GLP-1, GLP-2 and oxyntomodulin in the CNS: role of peripherally secreted and centrally produced peptides. Prog. Neurobiol 92, 442–462. 10.1016/j.pneurobio.2010.07.003. [PubMed: 20638440]

Weeber EJ, Beffert U, Jones C, Christian JM, Forster E, Sweatt JD, and Herz J (2002). Reelin and ApoE receptors cooperate to enhance hippocampal synaptic plasticity and learning. J. Biol. Chem 277, 39944–39952. 10.1074/jbc.M205147200. [PubMed: 12167620]

Whitlock JR, Heynen AJ, Shuler MG, and Bear MF (2006). Learning induces long-term potentiation in the hippocampus. Science 313, 1093–1097. 10.1126/science.1128134. [PubMed: 16931756]

Wu X, Ge H, Gupte J, Weiszmann J, Shimamoto G, Stevens J, Hawkins N, Lemon B, Shen W, Xu J, et al. (2007). Co-receptor requirements for fibroblast growth factor-19 signaling. J. Biol. Chem 282, 29069–29072. 10.1074/jbc.C700130200. [PubMed: 17711860]

Xu C, Messina A, Somm E, Miraoui H, Kinnunen T, Acierno J Jr., Niederländer NJ, Bouilly J, Dwyer AA, Sidis Y, et al. (2017). KLB, encoding β-Klotho, is mutated in patients with congenital hypogonadotropic hypogonadism. EMBO Mol. Med 9, 1379–1397. 10.15252/emmm.201607376. [PubMed: 28754744]

Xu J, Bartolome CL, Low CS, Yi X, Chien CH, Wang P, and Kong D (2018). Genetic identification of leptin neural circuits in energy and glucose homeostases. Nature 556, 505–509. 10.1038/s41586-018-0049-7. [PubMed: 29670283]

Yuan X, Zhou X, Chen Z, He Y, Kong Y, Ye S, Gao N, Zhang Z, Zhang H, and Li J (2019). Genome-wide DNA methylation analysis of hypothalamus during the onset of puberty in gilts. Front. Genet 10, 228. 10.3389/fgene.2019.00228. [PubMed: 30941164]

Highlights

- FGF21 is not produced from hypothalamic tanycytes
- Instead, FGF21 is expressed in the brain in the retrosplenial cortex
- Brain-derived FGF21 regulates memory formation but not metabolism
- FGF21 signaling to the hippocampus prolongs the duration of long-term potentiation

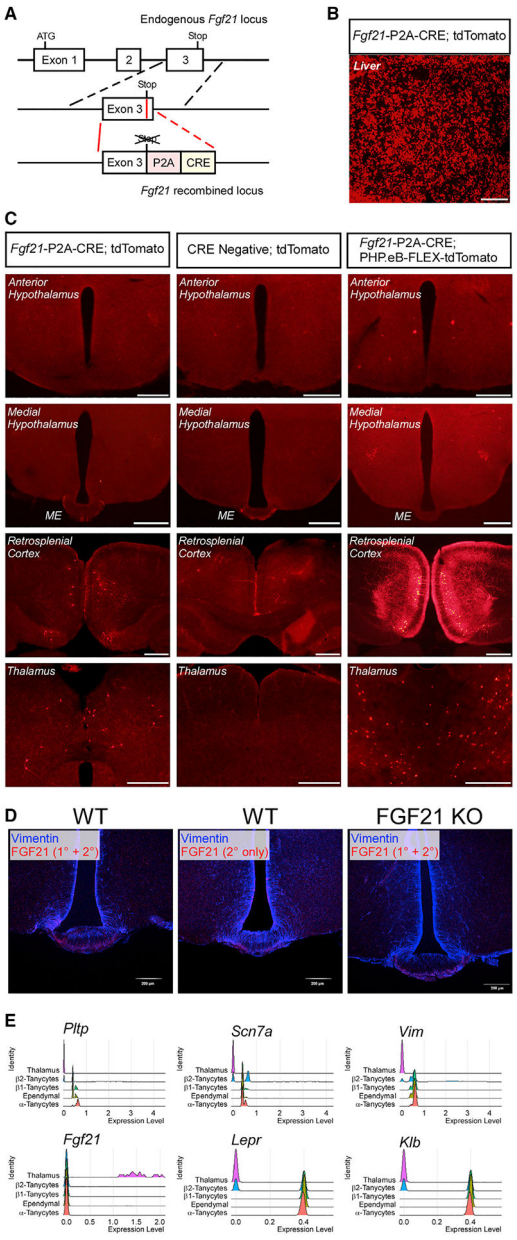

Figure 1. FGF21 is expressed in the cortex but not hypothalamic tanycytes

(A) Schematic representation of the targeting strategy of *Fgf21*-P2A-CRE mice. Solid lines represent chromosome sequence. CRE, CRE-re-combinase coding sequence; P2A, 2A self-cleaving peptide sequence.

(B) Representative fluorescence imaging for tdTomato-positive cells in the liver of 12-week-old male *Fgf21*-P2A-CRE; Ai14 tdTomato mice. Scale bar, 500 μm.

(C) Representative fluorescence imaging for tdTomato-positive cells in the anterior and medial hypothalamus, retrosplenial cortex (RSC) and thalamus of 8- to 12-week-old male *Fgf21*-P2A-CRE; Ai14 tdTomato, CRE negative; Ai14 tdTomato and *Fgf21*-P2A-CRE; PHP.eB-FLEX-tdTomato mice. Scale bar, 500 μm.

(D) Representative immunofluorescence imaging for FGF21 and vimentin in the median eminence of wild-type (WT) mice using primary and secondary or secondary only antibodies (Geller et al., 2019). Also included is a representative immunofluorescence image for FGF21 and vimentin in the median eminence of FGF21 knockout (KO) mice.
(E) Expression levels of phospholipid transfer protein (*Pltp*), sodium voltage-gated channel alpha subunit 7 (*Scn7a*), vimentin (*Vim*), *Fgf21,* leptin receptor (*Lepr*), and β-klotho (*Klb)* in thalamic cells, β2-tanycytes, β1-tanycytes, ependymal cells, and α-tanycytes (>5,000 cells all together) presented as a Ridge plot (where expression levels of single cells are plotted along the x axis and the height of the peaks on the y axis indicate the relative proportion of cells expressing the indicated transcripts at a given expression level) using deposited single-cell RNA-seq data.
See also Figure S1 and Video S1.

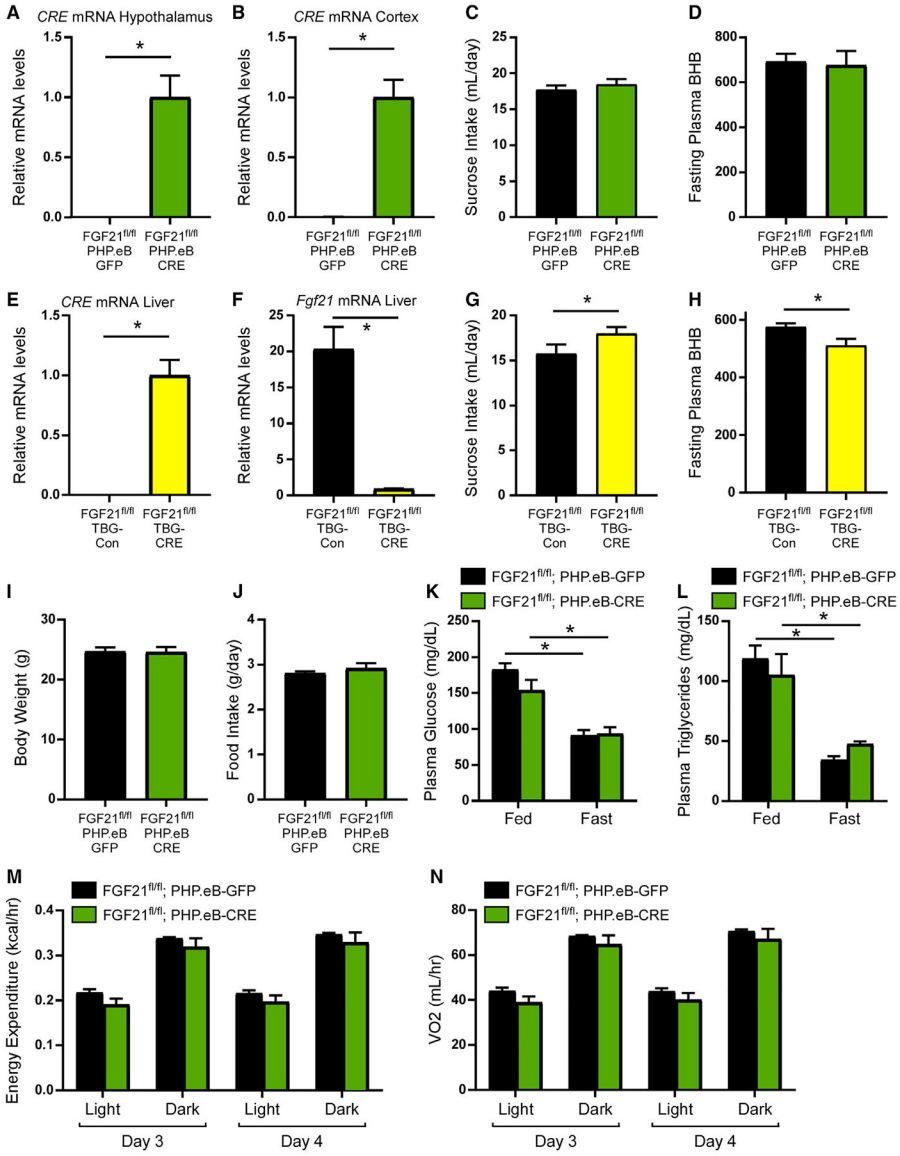

Figure 2. Endogenous hepatic FGF21, but not central FGF21, regulates sucrose consumption and hepatic metabolism

(A and B) Relative *CRE* mRNA levels in the hypothalamus (A) and retrosplenial cortex (B) of 12- to 14-week-old male FGF21$^{fl/fl}$ mice injected with PHP.eB-GFP or PHP.eB-CRE virus (n = 7–9/group). Statistical analyses were conducted using a two-tailed t test (*p < 0.05).

(C) Last 3 days average fluid intake during two-bottle choice of 10% sucrose versus water in 12- to 14-week-old male FGF21$^{fl/fl}$ mice injected with PHP.eB-GFP or PHP.eB-CRE virus (n = 9–10/group). Statistical analyses were conducted using a two-tailed t test.

(D) Plasma β-hydroxybutyrate (BHB) levels (μmol/L) after a 24-h fast in 12- to 14-week-old male FGF21$^{fl/fl}$ mice injected with PHP.eB-GFP or PHP.eB-CRE virus (n = 7/group). Statistical analyses were conducted using a two-tailed t test.

(E and F) Relative mRNA levels of *CRE* (E) and *Fgf21* (F) from the liver of 12- to 14-week-old male FGF21$^{fl/fl}$ mice injected with AAV-TBG-Con (null) or AAV-TBG-CRE

virus (n = 10/group). Statistical analyses were conducted using a two-tailed t test (*p < 0.05).

(G) Last 3 days average fluid intake during two-bottle choice of 10% sucrose versus water in 12- to 14-week-old male $FGF21^{fl/fl}$ mice injected with AAV-TBG-Con (null) or AAV-TBG-CRE virus (n = 10/group). Statistical analyses were conducted using a two-tailed t test (*p < 0.05).

(H) Plasma β-hydroxybutyrate (BHB) levels (μmol/L) after a 24-h fast in 12- to 14-week-old male $FGF21^{fl/fl}$ mice injected with AAV-TBG-Con (null) or AAV-TBG-CRE virus (n = 7–8/group). Statistical analyses were conducted using a two-tailed t test (*p < 0.05).

(I and J) Body weight (I) and average daily food intake (J) of 12- to 14-week-old male $FGF21^{fl/fl}$;PHP.eB-GFP and $FGF21^{fl/fl}$;PHP.eB-CRE mice fed *ad libitum*. Statistical analyses were conducted using a two-tailed t test.

(K and L) Plasma glucose (K) and plasma triglyceride (L) levels of 12- to 14-week-old male $FGF21^{fl/fl}$;PHP.eB-GFP and $FGF21^{fl/fl}$;PHP.eB-CRE mice either *ad libitum* fed or following a 24-h fast (n = 7–9/group). Statistical analyses were conducted using a two-way ANOVA with multiple comparisons (*p < 0.05).

(M and N) Energy expenditure (M) and oxygen consumption (VO_2) (N) of 12- to 14-week-old male, *ad libitum* fed $FGF21^{fl/fl}$;PHP.eB-GFP and $FGF21^{fl/fl}$;PHP.eB-CRE mice (n = 7–9/group) during day 3 and 4 in the metabolic chambers. Statistical analyses were conducted using a two-way ANOVA with multiple comparisons (*p < 0.05).

Values are mean ± SEM.

See also Figure S2.

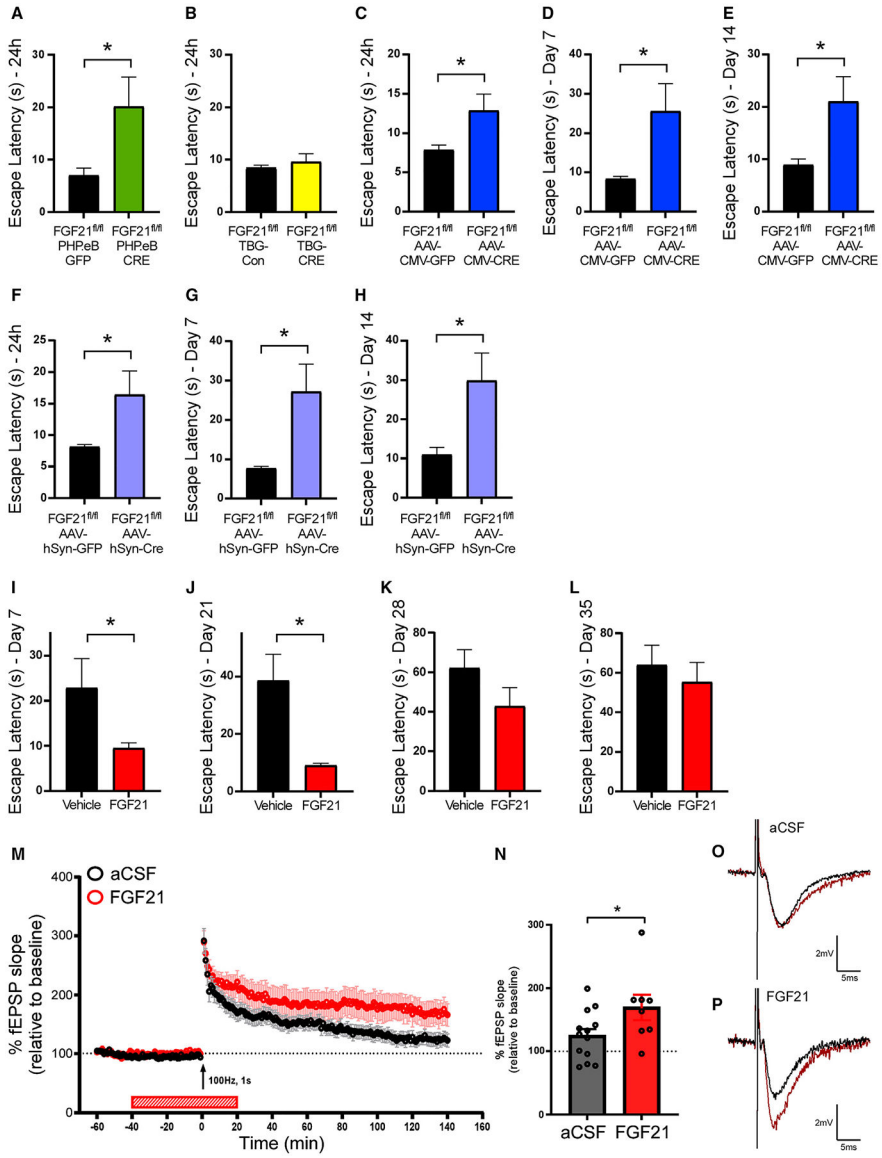

Figure 3. FGF21 regulates spatial learning and memory in mice

(A and B) Escape latency on test trials 24 h after training of male FGF21$^{fl/fl}$ mice injected with (A) PHP.eB-GFP or PHP.eB-CRE virus (n = 7–9/group) or (B) AAVTBG-Con (null) or AAV-TBG-CRE virus (n = 12–15/group). Statistical analyses were conducted using a two-tailed t test (*p < 0.05).

(C–E) Escape latency on test trials (C) 24 h, (D) 7 days, and (E) 14 days after training of 11- to 13-week-old male FGF21$^{fl/fl}$ mice injected with AAV-CMV-CRE or AAV-CMV-EGFP virus in the RSC (n = 14–15/group). Statistical analyses were conducted using a two-tailed t test (*p < 0.05).

(F–H) Escape latency on test trials (F) 24 h, (G) 7 days, and (H) 14 days after training of 11- to 13-week-old male FGF21$^{fl/fl}$ mice injected with AAV-hSyn-CRE-EGFP or control virus in the RSC (n = 16/group). Statistical analyses were conducted using a two-tailed t test (*p < 0.05).

(I–L) Escape latency on test trials (I) 7 days, (J) 21 days, (K) 28 days, and (L) 35 days after the training of 11- to 13-week-old male C57BL/6J mice treated with FGF21 (1 mg/kg) or saline for 4 days via IP injection (n = 14–15/group). Statistical analyses were conducted using a two-tailed t test (*p < 0.05).

(M) Long-term potentiation (LTP) was induced by a single 100-Hz, 1-second-duration stimuli (indicated by arrow). LTP maintenance was significantly enhanced in slices from C57BL/6J wild-type mice bath applied FGF21 (50 μg/mL in aCSF) compared with aCSF alone (n = 13 slices for aCSF prepared from 10 mice and eight slices for FGF21 prepared from eight mice).

(N) Average of fEPSP slope over final 20 min of LTP. Statistical analyses were conducted using a two-tailed t test (*p < 0.05).

(O and P) Representative traces of LTP recordings shown in (M).

Values are mean ± SEM (*p < 0.05).

See also Figures S3 and S4.

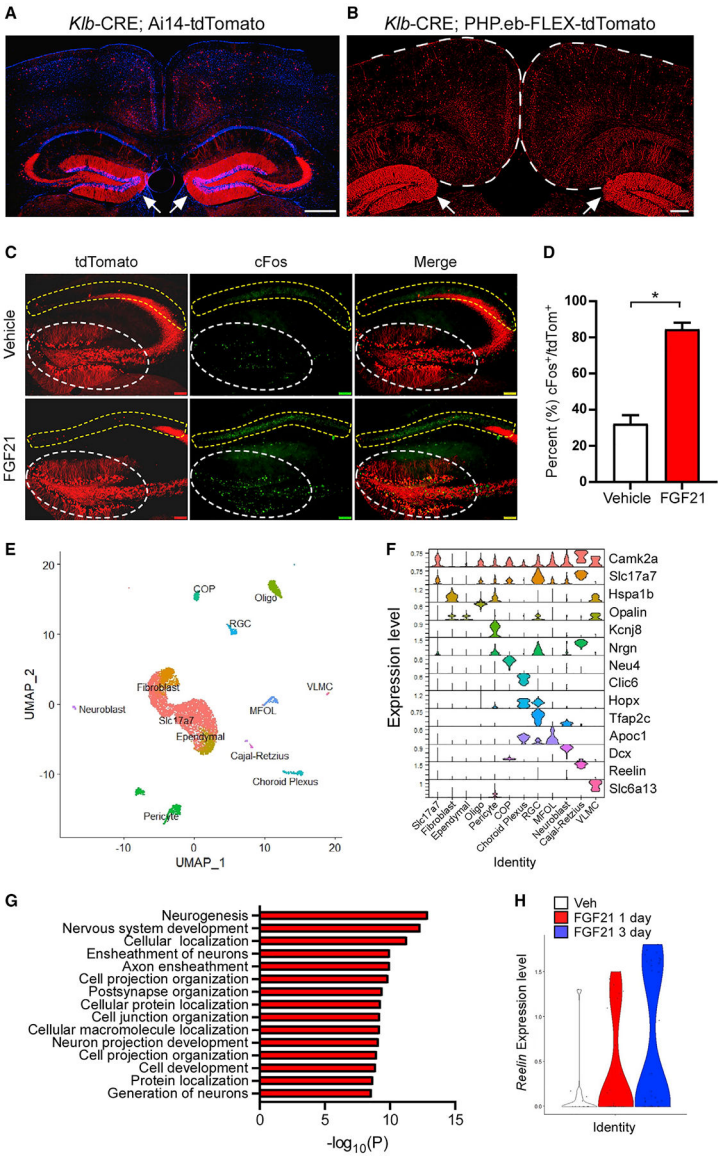

Figure 4. FGF21 signals to the hippocampus to modulate neuron activity and Reelin expression

(A and B) Representative fluorescence imaging of tdTomato-positive cells in the retrosplenial cortex and dentate gyrus of the hippocampus (white arrows) from male *Klb*-CRE; Ai14 tdTomato mice (A; scale bar, 500 μm) or *Klb*-CRE; PHP.eB-FLEX-tdTomato mice (B; scale bar, 200 μm).

(C) Immunofluorescence imaging for cFos in the hippocampus (dentate gyrus, white circle; CA1, yellow circle) of *Klb*-CRE; Ai14 tdTomato mice treated with vehicle or FGF21 (1 mg/kg) IP injection for 1 h.

(D) Percent of cFos-positive cells in KLB/tdTomato^{+} cells in the dentate gyrus from *Klb*-CRE; Ai14 tdTomato mice treated with vehicle or FGF21 (1 mg/kg) for 1 h (n = 3–4/group). Statistical analyses were conducted using a two-tailed t test (*p < 0.05).

(E) Single-cell RNA sequencing of tdTomato-expressing cells isolated from the dentate gyrus of *Klb*-CRE; Ai14-tdTomato mice and UMAP clustering to identify distinct cell types

(RGC, radial glia cell; COP, committed oligodendrocytes precursor; MFOL, myelin forming oligodendrocytes; VLMC, vascular lepotomeningeal cell; Slc17a7, vesicular glutamate transporter 1).

(F) A violin plot representation of the expression of genes that encode the indicated cell-type markers across clusters in tdTomato$^+$ cells isolated from the dentate gyrus of *Klb*-CRE; Ai14-tdTomato mice (RGC, radial glia cell; COP, committed oligodendrocytes precursor; MFOL, myelin forming oligodendrocytes; VLMC, vascular lepotomeningeal cell; Slc17a7, vesicular glutamate transporter 1).

(G) Gene ontology analysis of gene networks associated with biological processes and subcellular compartments significantly upregulated (p values on x axis) in dentate gyrus KLB$^+$ cells isolated from mice treated with FGF21 (1 mg/kg) for 3 days relative to mice treated with vehicle.

(H) Relative *Reelin* expression level in the dentate gyrus KLB$^+$ cells from mice treated with vehicle or FGF21 (1 mg/kg) for 1 day or 3 days. Values are mean ± SEM (*$p < 0.05$). Statistical analyses were conducted using an unpaired two-tailed t test or two-way ANOVA with multiple comparisons. Sidak's test was used for post hoc analysis of significant differences between the groups.

KEY RESOURCES TABLE

REAGENT or RESOURCE	SOURCE	IDENTIFIER
Antibodies		
Rabbit monoclonal FGF21 antibody	Abcam	Cat#: ab171941; RRID: AB_2629460
Chicken anti-Vimentin antibody	Millipore	Cat#: AB5733; RRID: AB_11212377
Alexa Fluor 594-AffiniPure F(ab')2 Fragment Donkey anti-Rabbit IgG (H+L)	Jackson ImmunoResearch Labs	Cat#: 711-586-152 RRID: AB_2340622
Alexa Fluor 647-AffiniPure F(ab')2 Fragment Donkey anti-Chicken IgY (IgG) (H+L)	Jackson ImmunoResearch Labs	Cat#: 703-606-155 RRID: AB_2340380
c-FOS (9F6) Rabbit mAb	Cell Signaling Technology	Cat#:2250; RRID: AB_2247211
F(ab')2-Goat anti-Rabbit IgG (H+L) Secondary Antibody, Alexa Fluor 488	Life Technologies	Cat#: A-11070
Goat anti-Chicken IgY (H+L) Secondary Antibody, Alexa Fluor 488	ThermoFisher Scientific	Cat#: A-11039
Goat anti-Rabbit IgG (H+L) Cross-Absorbed Secondary Antibody, Texas Red	ThermoFisher Scientific	Cat#: T-2767
Bacterial and virus strains		
pAAV-FLEX-tdTomato	Addgene	Cat#:28306-PHPeB, RRID:Addgene 28306
AAV9-CMV-Cre	VectorBuilder	Designed by lab
AAV9-CMV-GFP.WPRE	VectorBuilder	Designed by lab
pENN.AAV.hSyn.HI.eGFP-Cre.WPRE.SV40	Addgene	Cat#:105540-PHPeB RRID:Addgene 105540
AAV2/PHP.eBCMVeGFP	University of Iowa	N/A
AAV-CMV-GFP	Addgene	Cat#:67634, RRID:Addgene 67634
AAV.TBG.PI.Cre.rBG	Addgene	Cat#:107787-AAV8, RRID:Addgene 1077887
pAAV.TBG.PI.Null.bGH	Addgene	Cat#:105536-AAV8, RRID:Addgene 105536
pENN.AAV.hSyn.HI.eGFP-Cre.WPRE.SV40	Addgene	Cat#: 105540-AAV9 RRID:Addgene 105540
Chemicals, peptides, and recombinant proteins		
Recombinant Human FGF21	Novo Nordisk	N/A
NaCl	Sigma	Cat#: S9888
KCl	Sigma	Cat#: P3911
NaH_2PO_4	Sigma	Cat#: S0751
$CaCl_2.2H_2O$	Sigma	Cat#: 223506
$MgSO_4.7H_2O$	Sigma	Cat#: 230391
$NaHCO_3$	Sigma	Cat#: S6014
D-glucose	Sigma	Cat#: G8270
Actinomycin D	Sigma	Cat#: A1410
N-Methyl-D-glucamine	Sigma	Cat#: M2004
Thiourea	Sigma	Cat#: T8656
Sodium Pyruvate	Sigma	Cat#: P2256
HEPES	Research Products International	Cat#: H75030

REAGENT or RESOURCE	SOURCE	IDENTIFIER
Sodium Ascorbate	Research Products International	Cat#: S42175
Fetal Bovine Serum	GIBCO	Cat#: 26140–079
(±)–α–Tocopherol (Vitamin E) solution	Sigma	Cat#: V-020–1ML
Dichloromethane	Sigma	Cat#: 270997–1L
Benzyl alcohol, anhydrous, 99.8%	Sigma	Cat#: 305197–1L
Benzyl Benzoate	Sigma	Cat#: W213802
Diphenyl Ether	Sigma	Cat#: 240834
Tetrahydrofuran	Fisher Scientific	Cat#: AAL13304AP
triethylamine	Fisher Scientific	Cat#: O4885–1
Critical commercial assays		
Glucose Autokit	Wako Chemicals	439-90901
3-HB Autokit	Wako Chemicals	Cat#: NC0092299, NC0092301
Infinity™Triglyceride	Thermo Scientific	TR22421
Deposited data		
Processed scRNAseq data	Gene Expression Omnibus	GSE208083
Experimental models: Organisms/strains		
Ai14;tdTomato	The Jackson Laboratory	007914
C57BL/6J	The Jackson Laboratory	003548
$FGF21^{fl/fl}$	The Jackson Laboratory	022361
FGF21 KO	Dr. Steven Kliewer	033846
FGF21-P2A-Cre	This paper	N/A
Klb-CRE	(Jensen-Cody et al., 2020)	N/A
Oligonucleotides		
mU36B4 (F): 5'-CGTCCTCGTTGGAGTGACA-3′	This paper	N/A
mU36B4 (R): 5'-CGGTGCGTCAGGGATTG-3′	This paper	N/A
FGF21 (F): 5′-CCTCTAGGTTTCTTTGCCAACAG-3′	This paper	N/A
FGF21 (R): 5′-AAGCTGCAGGCCTCAGGAT-3′	This paper	N/A
CRE (F): 5′-TGTTGCCGCGCCATCTG-3′,	This paper	N/A
CRE (R): 5′-TTGCTTCAAAAATCCCTTCCA-3′	This paper	N/A
Software and algorithms		
ImageJ	ImageJ	https://imagej.nih.gov/ij/
Graphpad Prism 7	Graphpad	http://www.graphpad.com/scientific-software/prism/
Promethion	Sable Systems International	Cat#: 3721
Ethovision XT 11.5	Noldus	https://www.noldus.com/ethovision-xt
VideoFreeze	Med Associates, Inc	Cat#: SOF-843
pCLAMP	Molecular Devices	N/A
Clampfit 11.2	Molecular Devices	N/A
Seurat	Seurat	https://satijalab.org/seurat/
R	The R Project for Statistical Computing	https://www.r-project.org/
Other		

REAGENT or RESOURCE	SOURCE	IDENTIFIER
RNAscope Multiplex Fluorescent Reagent Kit V2	Advanced Cell Diagnostics, INC	Cat#: 323100
RNAscope Probe - Mm-Fgf21	Advanced Cell Diagnostics, INC	Cat#: 460931
RNAscope Probe – tdTomato-C2	Advanced Cell Diagnostics, INC	Cat#: 317041-C2
Chow	Teklad	2920x
sucrose	Sigma	Cat#: S0389
Mounting media with DAPI	Vector Laboratories	Cat#: H-1200
Triton X-100	Sigma	9002-93-1
Tissue-Tek Optimal Cutting Temperature (OCT) Compound	Sakura	4583
Microvet	Sarstedt	90-1091
Trizol	Invitrogen	15596026
High-Capacity cDNA Reverse Transcription Kit	Life Technologies	4368814
Citrate buffer	Abcam	N/A
Donkey serum	Millipore	3430610
4% PFA	Thermoscientific	198906
0.9% sodium chloride	Hospira, Inc	NDC 0409-7138-09
DPBS (10X)	Gibco	2070626
Isoflurane	Zoetis	N/A